RSC Advances

ROYAL SOCIETY
OF **CHEMISTRY**

www.rsc.org/advances

Journal Name

ARTICLE

Mesoporous silica coated $Gd_2(CO_3)_3$:Eu hollow nanospheres for simultaneous cell imaging and drug delivery

Yanli Wu[a], Xianzhu Xu[b], Xi Chen[a], Ruchun Yang[a], QiangXiao[a*], Yongxiu Li[c*]

In the present work, the mesoporous silica coated $Gd_2(CO_3)_3$:Eu hollow nanospheres ($Gd_2(CO_3)_3$:Eu@mSiO$_2$ HNSs) were successfully synthesized via a facial route and characterized by X-ray diffraction (XRD), transmission electron microscope (TEM), scanning electron microscope (SEM) infrared spectrometer (IR), Energy dispersive X-ray spectrum (EDS) and Brunauer-Emmet-Teller (BET) surface area analysis. The results indicate that the prepared monodispersed nanoparticles are hollow spheres with a 400 nm sphere core and 30 nm thick shell and have a narrow size distribution. In vitro cell imaging of the hollow nanosphere shows $Gd_2(CO_3)_3$:Eu@mSiO$_2$ HNSs were able to enter NCI-H460 lung cancer cells rapidly. The possibility of using the synthesized hollow nanospheres for magnetic resonance imaging was also demonstrated, and the hollow nanosphere displays a clear T_1-weighted effect and could potentially serve as a bimodal T_1-positive contrast agent .The drug loading and controlled release performance of $Gd_2(CO_3)_3$:Eu@mSiO$_2$ HNSs was evaluated with Doxorubicin hydrochloride (DOX) as a model drug at different pH values (pH =7.4, 5.8). The $Gd_2(CO_3)_3$:Eu @mSiO$_2$ HNSs showed sustainable pH dependent drug release property. Furthermore, the in vitro cytotoxic effect against NCI-H460 Lung cancer cells of the DOX-loaded Carriers was investigated in detail. In all, The $Gd_2(CO_3)_3$:Eu @mSiO$_2$ HNSs as a new type of theragnostic (imaging and treatment) agent can provide new opportunities in cancer treatment.

Introduction

The design and synthesis of multifunctional nanomedical platforms that integrate suitable multiple nanomaterials with different properties into one single nanosystem provides an unparalleled opportunity for the simultaneous diagnostics and therapy of diseases.[1-3] For example, hollow multifunctional nanomaterials with low densities and high surface–to-volume ratios have been used for drug delivery to improve therapeutic efficiency and reduce toxicity.[4-7] Hollow structures have gained particular attentions in the field of drug storage and release because of their

large voids inside the shells and mesopores in the shells.[8] The large voids can store more drug molecules than the conventional mesoporous materials, and the mesopores in the shells provide accessible channels for drug molecule diffusion and mass transfer without blocking. It is worth noting that the multimodal mesoporous nanoparticles suitable for optical, magnetic resonance (MRI) imaging, and drug delivery can be realized by the hollow and mesoporous drug delivery system by incorporating multiple imaging probes. [9-13] The multimodal mesoporous nanoparticles are of great interest because they ally the highly sensitive fluorescence imaging and the high spatial resolution of MRI with controlled drug release.

In recent years, much research attention has been paid to the rare earth ions doped Gd-based nanocrystals due to their unique magnetic and optical characteristics arising from their 4f electrons. Highly water-dispersible Gd-based nanoparticles, such as $GdPO_4$[14-17], $NaGdF_4$[18,19], and Gd_2O_3[20,21], have been reported as the doping matrices of luminescent ions (Eu^{3+}, Tb^{3+}, Yb^{3+}/Er^{3+}) and magnetic ions (Gd^{3+}) that possess seven unpaired electrons and can efficiently alter the relaxation time of the surrounding water protons. However, their cytotoxicity has been rarely discussed. Recently, Fosrenol (lanthanum carbonate, $La_2(CO_3)_3$) has been approved as a phosphate binder for the treatment of hyperphosphatemia in renal dialysis patients in both USA and Europe [22], indicating the promising biological application prospect of $Gd_2(CO_3)_3$ [23, 24]. In our previous work, the rare earth ions doped $Gd_2(CO_3)_3$ nanoparticles were prepared by a reverse microemulsion method, and used as the dual modal agent for optical and magnetic resonance imaging [24]. The chemical similarities of lanthanide elements indicate that the rare earth ions doped $Gd_2(CO_3)_3$ nanoparticles might be safe for clinical applications. Therefore, it is expected that the hollow-structured $Gd_2(CO_3)_3$ would provide more space for drug loading due to the hollow spherical core and nanopore channels and thus it is more attractive than the conventional $Gd_2(CO_3)_3$ nanoparticles. And so far, there is no report on preparing hollow structured $Gd_2(CO_3)_3$:Eu for biomedical application.

Many efforts have been made to develop efficient methods for the design and preparation of hollow nanostructures during the past decade. Template-directed synthesis method has been demonstrated to be an effective approach to prepare inorganic hollow spheres. Hard templates, such as polymer latex particles and carbon spheres and silica, [25, 26] and soft templates, such as emulsion droplets, micelles, and gas bubbles, [27-29] are the two kinds of templates widely used in the template-directed synthesis method.

In the present work, we have developed a new strategy for the fabrication of mesoporous silica coated $Gd_2(CO_3)_3$:Eu hollow nanospheres ($Gd_2(CO_3)_3$:Eu @mSiO$_2$ HNSs, scheme 1). The hollow nanospheres were prepared by a homogeneous precipitation method using urea as a precipitating agent and silica nanosphere as a hard template, followed by a NaOH etching treatment. The hollow nanospheres were subsequently coated with a thin layer of silica and refluxed to remove the directing agent CTAB for the pore evolution and channel formation. The structure, formation process, luminescence and paramagnetic properties of the as-obtained nanostructure were investigated in detail. In addition, the high drug loading capacity and controlled drug release property of the prepared hollow-structured nanoparticles were demonstrated with Doxorubicin hydrochloride (DOX) as a model drug.
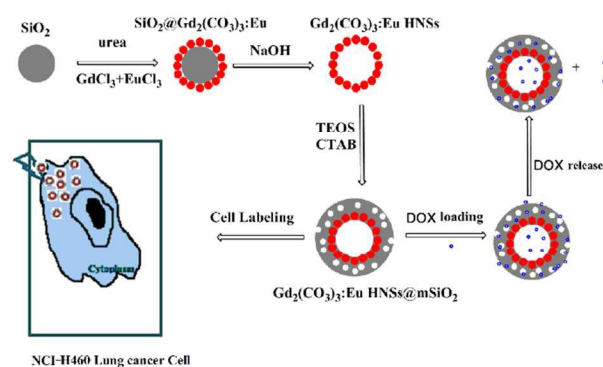
Scheme 1. Schematic illustration of the synthesis of $Gd_2(CO_3)_3$:Eu @mSiO$_2$ HNSs

Experimental

Materials

Materials. Gd_2O_3 (99.99%), Eu_2O_3 (99.99%), tetraethyl orthosilicate (TEOS) (99.0 %), and $RECl_3$ (RE=Gd and Eu) salts were freshly prepared by the reaction of RE_2O_3 with dilute hydrocholic acid. All other chemicals were of analytical-grade and used as received without further purification.

Synthesis of silica cores

The highly monodispersed silica nanospheres (NSs) were synthesized by a modified Stőber method [30, 31]. The hydrolysis of tetraethoxysilane (TEOS) by ammonia in an ethanol/water solution yields the colloidal solution of silica nanoparticles with a narrow size distribution under optimal conditions. In a typical preparation, the mixture of 3 mL TEOS and 47 mL EtOH was added to a 50 mL ammonia solution in $EtOH/H_2O$ with a $NH_3.H_2O$ (25 wt %):H_2O:EtOH volume ratio of 5:10:35 and stirred at room temperature for 5 h to form a white silica colloidal suspension. The silica particles were collected by centrifugation and washed with ethanol four times. The particle size of SiO_2 naonospheres were tuned by adjusting the amount of TEOS.

Synthesis of core-shell $SiO_2@Gd_2(CO_3)_3$:Eu NPs

To prepare core-shell $SiO_2@Gd_2(CO_3)_3$:Eu nanoparticles, 9.5 mmol $GdCl_3$ and 0.5 mmol $EuCl_3$ were dissolved in 200 mL distilled water and then mixed with 3.0 g urea and 3.0 g PVP under vigorous stirring to form a clear solution. The as-prepared SiO_2 nanospheres (400 mg) were well-dispersed in the above solution with the assistance of 10 mins ultrasonication. The SiO_2 nanosphere suspension was transferred into a 500 mL round-bottom flask and heated at 90 °C for 6 h under vigorous stirring. The produced core-shell product was collected by centrifugation and washed with distilled water and ethanol for three times, respectively, and dried at 60 °C.

Synthesis of $Gd_2(CO_3)_3$:Eu HNSs

The as-prepared core-shell structured $SiO_2@Gd_2(CO_3)_3$:Eu NPs (600 mg) was added to 20 mL 15 % NaOH and stirred overnight to remove the SiO_2 core. The hollow $Gd_2(CO_3)_3$:Eu NSs were washed with distilled water several times for further use.

Synthesis of $Gd_2(CO_3)_3$:Eu @$mSiO_2$ HNSs

The precursor of $Gd_2(CO_3)_3$:Eu HNs was then coated with a silica layer by a modified Stöber process. The prepared $Gd_2(CO_3)_3$:Eu HNSs (300 mg) were dispersed in 200 mL solution containing CTAB (300 mg) in $EtOH-H_2O$ solution (v/v, 160/40) under ultrasonication. One milliliter 25 % ammonia and 300 μg TEOS were subsequently added to the $Gd_2(CO_3)_3$:Eu HNSs suspension dropwise and stirred at room temperature for 12 h. The nanoparticles were collected by centrifugation, sequentially washed with deionized water and EtOH, and dried at 60 °C. The directing agent (CTAB) was extracted from the $Gd_2(CO_3)_3$:Eu hollow nanospheres as described in the previous report[32]. The dense silica coated precursor (200 mg) was dispersed in 50 mL acetone and refluxed at 75 °C for 10 h. The CTAB-removed product was collected by centrifugation, washed with acetone twice, and dried at 80 °C for 12 h. The product was denoted as $Gd_2(CO_3)_3$:Eu@$mSiO_2$.

Characterization

The X-ray diffractions (XRD) of the powder samples were examined on a diffractometer (D8 Advance, Bruker, Germany). The morphologies of the products were imaged with a scanning electron microscopy (Quanta 200F, FEI, Hillsboro, USA) equipped with Energy dispersive X-ray spectrometer (GENESIS, EDAX, USA) and a transmission electron microscopy (Tecnai G20, FEI, Hillsboro, USA) equipped with a field emission gun operating at 200 kV. IR spectra were recorded on a Perkin–Elmer C99957 IR spectrophotometer (Perkin–Elmer, USA). The N_2 adsorption/desorption isotherm was measured with a Micromeritics ASAP 2010M instrument at liquid nitrogen temperature (77 K). The specific surface area was determined by the Brunauer-Emmett-Teller (BET) method. Dynamic light scattering (DLS) measurements were carried out using a particle size analyzer (NPA152, Microtrac, USA). Photoluminescence was examined

under an F4500 fluorescent spectroscopy (Hitachi, Japan) and magnetic measurements were carried out with a vibrating sample magnetometer in the range from -20 to 20 kOe (MPMS XL-7, Quantum Design Inc, USA). The Absorption spectra were obtained with an UV/VIS spectrometer （Agilent 8453，USA）.

Cell imaging

NCI-H460 Lung cancer cells were plated on 14 mm glass coverslips, allowed to adhere for 24 h, washed with phosphate buffer solution (PBS), and incubated in a serum-free cell culture medium containing 100 μg.mL^{-1} $Gd_2(CO_3)_3$:Eu@mSiO$_2$ HNSs at 37 °C under 5 % CO$_2$ for 4 h. The excessive nanoparticles were removed by sufficiently washing the cells with PBS. Fluorescence images of the cells were collected on a confocal microscopy (ZEISS 710, Zeiss, Germany) under excitation at 405 nm.

In vitro T$_1$-weighted MRI and longitudinal relaxivity

The T$_1$-weighted MR images were obtained using a 0.5 T magnet (Shanghai Niumag Corporation NM 120-Analyst). The r_1 was calculated according to the equation $r_1=\Delta R_1/[Gd^{3+}$ concentration, where R_1 was the longitudinal relaxation rate $(R_1=1/T_1$, unit of s^{-1}). In this study, R_1 values of Gd^{3+} with different concentrations (0–1.0 mM^{-1}) .

Drug loading and drug release

Doxorubicin hydrochloride (DOX), a typical antitumor drug, was used as a model drug to evaluated the drug loading and controlled release performance of $Gd_2(CO_3)_3$:Eu @mSiO$_2$ HNSs. Briefly, 10 mg of as-prepared $Gd_2(CO_3)_3$:Eu @mSiO$_2$ HNSs was dispersed in 4 mL of PBS (pH = 7.4) with a DOX concentration of 0.5 mg.mL^{-1}. The DOX loaded $Gd_2(CO_3)_3$:Eu@mSiO$_2$ HNSs sample was collected by centrifugation. To evaluate the DOX loading amount, the supernatant solution was collected, and the content of residual DOX was determined by UV−vis measurement at a wavelength of 480 nm, as shown in Figure S3. Supplementary Information.

The in vitro delivery test was performed by immersing the DOX -loaded $Gd_2(CO_3)_3$:Eu @mSiO$_2$ sample in 4 mL of PBS. At predetermined time intervals, PBS was quickly taken and replaced with an equal volume of fresh PBS. The amount of released DOX in the supernatant solution was measured by UV-vis spectrophotometer, the supernatant and washed solutions were collected and the residual DOX content（R_{Dox}）was obtained by UV−vis measurement at 480 nm. The loading efficiency of DOX can be calculated as follows: [(O_{Dox} -R_{Dox})/O_{Dox}] *100%, in which O_{Dox} is the original DOX content.

In vitro cytotoxicity against NCI-H460 Lung cancer cells with free DOX and DOX-loaded $Gd_2(CO_3)_3$:Eu @mSiO$_2$

Lung cancer cells were plated out in 96-well plates at a density of 8000 cells per well and were allowed to the well for 24 h. The free DOX, DOX-loaded $Gd_2(CO_3)_3$:Eu @mSiO$_2$ were added to the medium, the cells were incubated in 5% CO$_2$ at 37 °C for 24 h. The concentrations of DOX were 0, 3.125, 6.25, 12.5, 25, and 50 μg mL^{-1}, respectively. Finally, the cell viability was evaluated by MTT (3-(4,5-dimethylthiazol-2-yl)-2,5-diphenyltetrazolium bromide) assay.

Biocompatibility of the $Gd_2(CO_3)_3$:Eu @mSiO$_2$ HNSs

The biocompatibility of the $Gd_2(CO_3)_3$:Eu @mSiO$_2$ HNSs was assessed by the standard MTT assay. The typical procedure and results were showed in Supplementary information.

3. Results and discussion

3.1 Formation Process, Phase Identification, and Morphology

The morphology and structure of the samples were characterized by SEM, TEM, XRD, and EDS. Figure. 1 shows the SEM images of silica NSs, core-shell-structured SiO$_2$@Gd$_2$(CO$_3$)$_3$:Eu, and the Gd$_2$(CO$_3$)$_3$:Eu HNSs. Figure. 2 shows the TEM images of core-shell-structured SiO$_2$@Gd$_2$(CO$_3$)$_3$:Eu, Gd$_2$(CO$_3$)$_3$:Eu HNSs, and Gd$_2$(CO$_3$)$_3$:Eu@mSiO$_2$ HNSs, and the HRTEM of the Gd$_2$(CO$_3$)$_3$:Eu @mSiO$_2$ HNSs. It is clear that silica NSs are uniform and monodisperse nanoparticles with smooth surfaces and an average diameter of 400 nm (Figure. 1a). It is noted that the uniform core-shell-structured SiO$_2$@Gd$_2$(CO$_3$)$_3$:Eu nanospheres inherited the spherical morphology and good dispersibility of the

silica templates. However, their surfaces are much rougher than that of the silica template due to core-shell-structure formed by the precipitation of a large number of uniform nanoparticles (Figure. 1b). Their panoramic SEM image indicates that $Gd_2(CO_3)_3$:Eu HNSs are well-dispersed hollow nanospheres with diameters of ~400 nm (Figure. 1c). These results reveal that the shape and structure of the final products essentially depend on the silica template.

The TEM image of core-shell-structured $SiO_2@Gd_2(CO_3)_3$:Eu (Figure. 2a) further shows the rough surfaces and solid structure of the precursor nanospheres with a diameter of 400 nm, consistent with the SEM result (Figure. 1b). The TEM image of the $Gd_2(CO_3)_3$:Eu HNSs (Fig 2b) indicates their uniform spherical morphology. The strong contrast between the dark edge and the pale center is the direct evidence for the hollow structure of the nanospheres. The Figure. 2c show that the $Gd_2(CO_3)_3$:Eu@mSiO$_2$ HNSs inherit the spherical morphology with diameter of about 400 nm and good dispersity of the precursor which was also identified by the DLS (as shown in Figure. S1. Supplementary information). HRTEM images of the mesoporous silica coated $Gd_2(CO_3)_3$: Eu clearly demonstrate that a 30 nm layer of silica has been successfully coated on the hollow nanosphere (Figure. 2d).
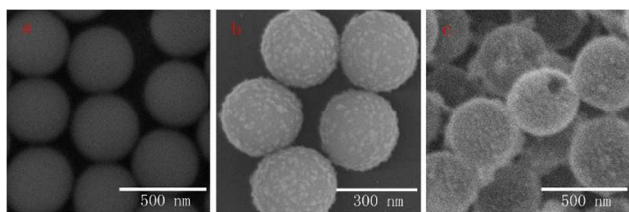
Figure 1 SEM images of pure SiO_2 (a), core-shell-structured $SiO_2@Gd_2(CO_3)_3$:Eu(b), and $Gd_2(CO_3)_3$:Eu HNSs (c).
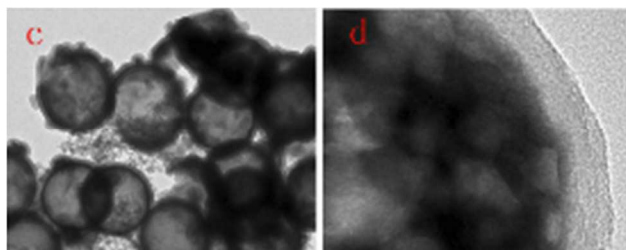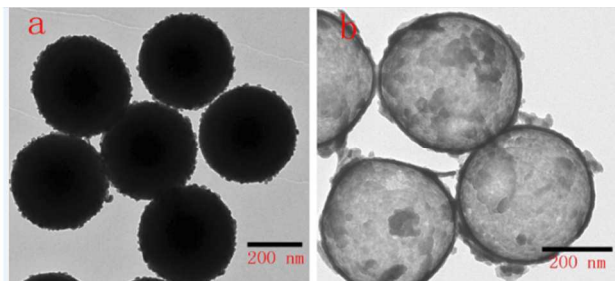
Figure 2 TEM images of core-shell-structured SiO_2 @ $Gd_2(CO_3)_3$:Eu (a), $Gd_2(CO_3)_3$:Eu HNSs (b), and $Gd_2(CO_3)_3$:Eu@mSiO$_2$ HNSs (c), and the HRTEM image of $Gd_2(CO_3)_3$:Eu @mSiO$_2$ HNSs (d)

The as-prepared $Gd_2(CO_3)_3$:Eu^{3+} HNSs showed no detectable XRD pattern (as shown in Figure S2. Supplementary information), indicating that the product is amorphous. EDS analysis results were showed in Figure.3 There were only two element peaks corresponding to Si and O in the curve a, no other impurity elements are found, that was consistent with the pure SiO_2. Excepted the element of Si and O, the Gd and Eu was found in the cure b, which should be ascribed to the core-shell structured $SiO_2@Gd_2(CO_3)_3$:Eu. The element peak of Si was almost disappeared and the peak intensity of the Gd, Eu ,C and O increased obviously for the hollow $Gd_2(CO_3)_3$:Eu,. Comparing the curve c and d, the peak of Si reappeared, that indicated the mesoporous silica was successfully coated onto the surface of the $Gd_2(CO_3)_3$:Eu HNSs.
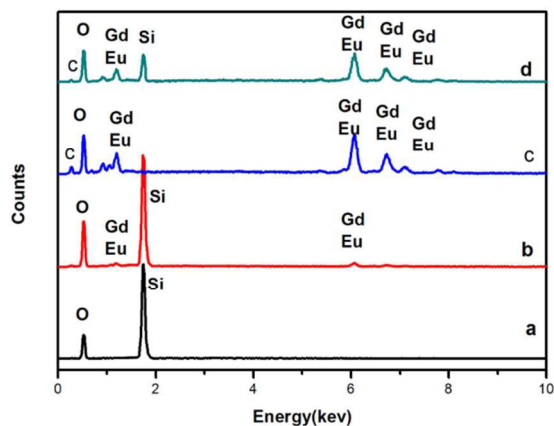
Figure 3 EDS spectrum of the samples: SiO_2 (a), core-shell-structured $SiO_2@Gd_2(CO_3)_3$:Eu(b), $Gd_2(CO_3)_3$:Eu HNSs (c), $Gd_2(CO_3)_3$:Eu@mSiO_2 HNSs (d)

IR spectroscopy was carried out to further examine the chemical compositions of the nanoparticle samples (Figure. 4). In the IR spectrum of the as-prepared SiO_2 nanospheres, the absorption bands due to OH (3420 cm^{-1}), H_2O (1634 cm^{-1}), Si-O-Si (v_{as}, 1080 cm^{-1}; v_s, 796 cm^{-1}), and Si-OH (v_s, 950 cm^{-1}) (where v_{as}= asymmetric stretching, v_s =symmetric stretching bending) were observed (Figure. 4a). In the Figure.4b for the core-shell structured $SiO_2@Gd_2(CO_3)_3$:Eu, in addition to the strong absorption band of Si-O-Si (v_{as}, 1080 cm^{-1}), two absorption bands at 1509 cm^{-1} and 1406 cm^{-1} appeared, which were ascribed to the bands of v_{as} O-C-O. This indicates the presence of the carbonate group. In the Figure. 4c for the hollow $Gd_2(CO_3)_3$:Eu, the characteristic bands of Si-O-Si (v_{as}, 1080 cm^{-1}) and Si-OH (v_s, 950 cm^{-1}) almost disappeared, the absorption bands of O-H (3420 cm^{-1}), O-C-O (1509 and 1406 cm^{-1}), C-O (1086 cm^{-1}) and p-CO$_3$ (856 cm^{-1}) were observed. For the $Gd_2(CO_3)_3$:Eu @mSiO_2 HNSs, the characteristic bands of Si-O-Si (v_{as}, 1080 cm^{-1}) and Si-OH (v_s, 950 cm^{-1}) appeared again (Figure. 4d).
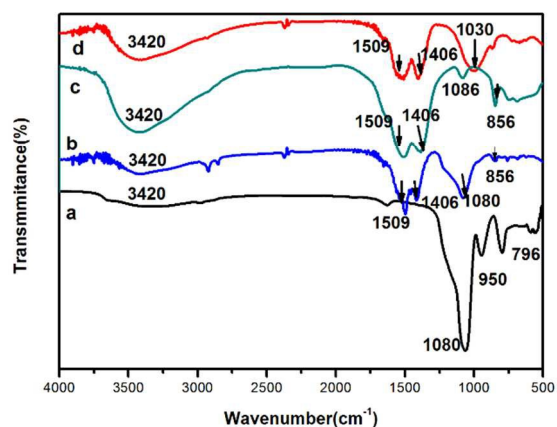
Figure 4 IR spectra of pure SiO_2 NSs (a), $SiO_2@Gd_2(CO_3)_3$:Eu (b), $Gd_2(CO_3)_3$:Eu HNSs (c) , and $Gd_2(CO_3)_3$:Eu@mSiO_2 HNSs (d)

The IR results indicate that the formation of $Gd_2(CO_3)_3$:Eu@mSiO_2 HNSs were subjected to four steps (scheme 1). First, highly monodispersed SiO_2 nanospheres were prepared by a modified Stöber method. Core-shell structured precursors were then produced by a homogeneous precipitation method using the

silica nanospheres as the template and urea as the precipitation agent. Urea played a crucial role in the formation of the precursor shell on the surface of the silica nanospheres. The decomposition of urea slowly released precipitating anions (mainly OH$^-$ and CO_3^{2-}) to the reaction systems at elevated temperature. And the precipitating anions dispersed on the surface of the silica sphere, so the Gd^{3+} and $Eu^{3+}$are easily to adsorb on the silica core, resulting in the homogeneous precipitation of the uniform precursor nanoparticles ($Gd_2(CO_3)_3$:Eu) coated on the surface of the silica template. The silica core was then removed with NaOH to produce $Gd_2(CO_3)_3$:Eu HNSs. A mesoporous silica layer was then coated on the surfaces $Gd_2(CO_3)_3$: Eu HNSs with CTAB as an organic template that was removed later to form $Gd_2(CO_3)_3$:Eu@mSiO_2 HNSs. Detailed experimental processes are given in the experimental section.

The specific surface area and porosity of $Gd_2(CO_3)_3$:Eu @mSiO_2 HNSs were determined by nitrogen adsorption method. The synthesised $Gd_2(CO_3)_3$:Eu @mSiO_2 HNSs showed a typical IV-type adsorption-desorption isotherm with a H_1-hysteresis loop, suggesting its mesoporous structure (Figure. 5). The BET surface area and total pore volume of $Gd_2(CO_3)_3$:Eu @mSiO_2 HNSs were calculated as 143.17 m^2.g^{-1} and 0.128 cm^3.g^{-1}, respectively.The pore-size distribution shows a narrow apex centered at 3.9 nm. These results evidently show the mesopore channels and large pore volume of the as-prepared $Gd_2(CO_3)_3$:Eu @mSiO_2 HNSs.
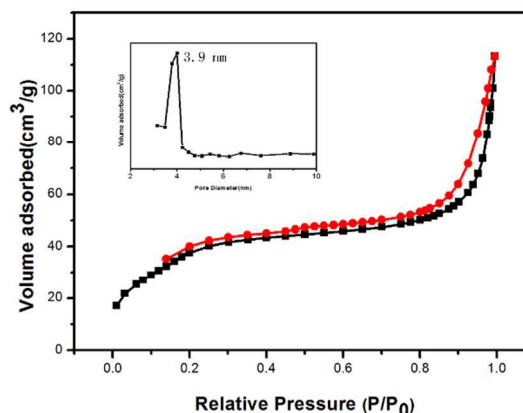
Figure 5 N_2 adsorption-desorption isotherms and mesopore size distribution (the inset) of the synthesized $Gd_2(CO_3)_3$:Eu @mSiO_2

Optical properties

Figure. 6 shows the excitation and emission spectra of the as-prepared $Gd_2(CO_3)_3$:Eu@mSiO$_2$ HNSs. The broad excitation band with a maximum at 254 nm was attributed to the charge transfer transition from europium to oxygen (CTB of Eu→O) (Fig. 6a). The weak lines between 300 and 500 nm can be ascribed to the characteristic f–f transitions of Eu^{3+} within its $4f^6$ configuration. The relatively stronger peaks were found at 395 nm ($^7F_0\rightarrow^5L_6$) and 466 nm ($^7F_0\rightarrow^5D_2$). Figure. 6b shows emission spectrum of the as-prepared $Gd_2(CO_3)_3$:Eu@mSiO$_2$ HNSs under the UV excitation at 395 at room temperature. The emission spectrum is composed of $^5D_0\rightarrow^7F_J$ (J =1, 2, 3, 4) transition lines of Eu^{3+} with the prominent peak of the $^5D_0 \rightarrow^7F_2$ hypersensitive transition at 613 nm under the excitation at 395 nm. As the digital photo shown in the inset of Figure. 6b, the HNSs in EtOH exhibit bright red luminescence under UV excitation.
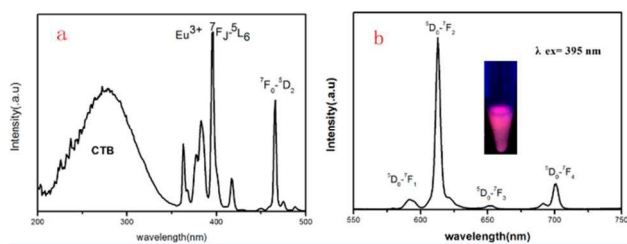
Figure.6 Excitation (a) and emission spectra (b) of $Gd_2(CO_3)_3$:Eu@mSiO$_2$ HNSs

Cell imaging

The application of $Gd_2(CO_3)_3$:Eu @mSiO$_2$ HNSs in the luminescence imaging of living cells was explored with NCI-H460 lung cancer cells. NCI-H460 lung cancer cells were incubated in a serum-free medium containing 100 μg.mL^{-1} $Gd_2(CO_3)_3$:Eu @mSiO$_2$ HNSs at 37 °C for 4 h and examined under a confocal fluorescence microscopy. Red fluorescence was observed on the $Gd_2(CO_3)_3$:Eu@mSiO$_2$ HNSs treated cells under an excitation at 405 nm (Figure. 7a). The labeling of cells was confirmed with the phase contrast (Figure.7b) and overlay (Figure. 7c) images. These results suggest that the $Gd_2(CO_3)_3$:Eu@mSiO$_2$ HNSs are able to enter living NCI-H460 lung cancer cells and can be used for cell imaging.
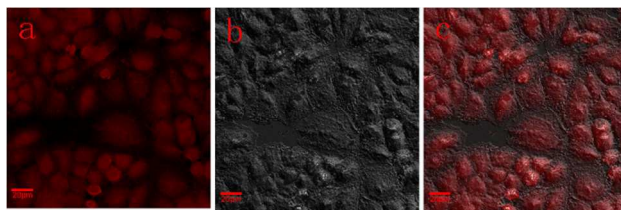
Figure 7 The confocal fluorescence (a), phase contrast (b), and overlay (c) images of NCI-H460 lung cancer cells exposed to $Gd_2(CO_3)_3$:Eu@mSiO$_2$ HNSs for 4 h

Magnetic and MRI studies

The magnetic property of the as-prepared $Gd_2(CO_3)_3$:Eu@mSiO$_2$ sample was determined with a magnetic property measurement system (MPMS XL-7). The plot of magnetization versus applied magnetic field for $Gd_2(CO_3)_3$:Eu @mSiO$_2$ HNSs was shown in Figure. 8. It showed the magnetization linearly increased with the increase of the applied magnetic field strength, indicating that the as prepared $Gd_2(CO_3)_3$:Eu@mSiO$_2$ HNSs possessed paramagnetism due to the seven unpaired inner 4f electrons of Gd^{3+} ions and is a promising candidate of MRI contrast agent. Figure. 9 shows the respective T_1-weighted images with a series of different Gd^{3+} concentrations (0.0, 0.2, 0.4, 0.5, 1.0 mM).The T_1-weighted images gradually became brighter, which accounts for positive enhancement of the effect on T_1-weighted sequences. The relaxation (r_1) value of the sample calculated from the slope of the concentration dependent relaxation T_1^{-1}, was estimated to be 1.15 mM^{-1}. S^{-1}. All of these results reveals the potential use of the $Gd_2(CO_3)_3$:Eu @mSiO$_2$ HNSs as an effective T_1 contrast agent.
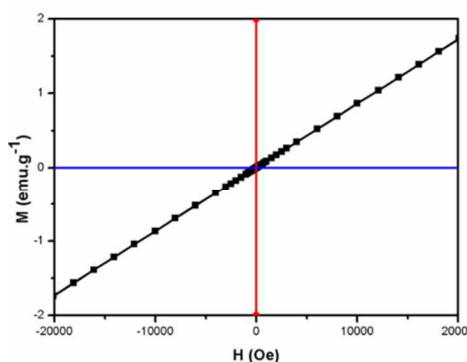
Figure. 8 The plot of magnetization versus applied magnetic field for $Gd_2(CO_3)_3$:Eu @mSiO_2 HNSs

Drug adsorption and release properties

DOX was selected as a model drug to determine the drug storage and release properties of DOX loaded $Gd_2(CO_3)_3$:Eu@mSiO_2 HNSs. The drug loading amount was calculated to be 93.3 μg/mg $Gd_2(CO_3)_3$:Eu@mSiO_2 HNSs. The drug releasing behavior of DOX-loaded particles was evaluated in PBS of two different pH values (7.4 and 5.8) . Figure. 10 shows the cumulative DOX release profile of the DOX loaded $Gd_2(CO_3)_3$:Eu@mSiO_2 in PBS as a function of release time. The drug release rate of the DOX loaded $Gd_2(CO_3)_3$:Eu@mSiO_2 was obviously pH dependent. Only 38.5 % is released after 24 h when pH=7.4. The release amount reached to 54.8% with the pH value decreased to 5.8 This trend may be explained by the increasing hydrophilicity and high solubility of DOX in the low pH[34] Considering the different pH value in blood (7.4), especially cancer tissue is acidic extracellular (5.8-7.2), the pH-sensitive drug release property is beneficial to targeting cancer tissues and reducing toxic side effect for normal tissues.
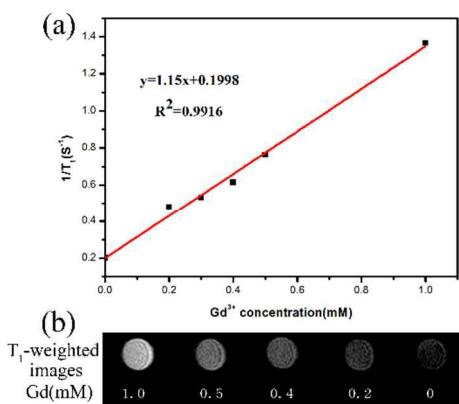
Figure. 9 Plots of $r1$（a）and T1 weighted MR images (b)
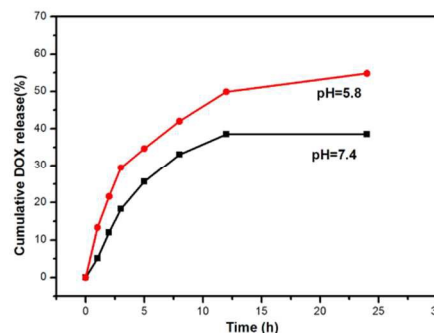
Figure 10 Cumulative DOX release of Dox loaded-$Gd_2(CO_3)_3$:Eu@mSiO_2 HNSs

In vitro cytotoxicity

In vitro cytotoxicity effects of the DOX and DOX loaded $Gd_2(CO_3)_3$:Eu@mSiO_2 HNSs were tested on NCI-H460 lung cancer cells via MTT assay. The concentrations of the free DOX and the DOX content in the DOX loaded $Gd_2(CO_3)_3$:Eu@mSiO_2 HNSs were 0, 3.125, 6.25, 12.5, 25, 50 μg mL^{-1}, respectively. As shown in Figure.11, both free DOX and DOX loaded $Gd_2(CO_3)_3$:Eu@mSiO_2 HNSs exhibited an increasing inhibition against NCI-H460 cells with the concentration increasing. At lower concentration, free DOX shows higher cytotoxicity than the DOX loaded $Gd_2(CO_3)_3$:Eu@mSiO_2 HNSs, but when the concentration increased to 25 μg.mL^{-1} similar cytotoxicity was founded. That can be ascribed to the sustainable release behavior of the DOX loaded $Gd_2(CO_3)_3$:Eu@mSiO_2 HNSs. In addition, MTT assay (Figure. S4, Supplementary information) demonstrates the satisfactory biocompatibility of the $Gd_2(CO_3)_3$:Eu@mSiO_2 HNSs, indicating that the nontoxic property of the sample. Based on these results, the $Gd_2(CO_3)_3$:Eu@mSiO_2 HNSs can potentially be used as anti-cancer drugs carrier and enhance the anti-cancer drug delivery efficacy.
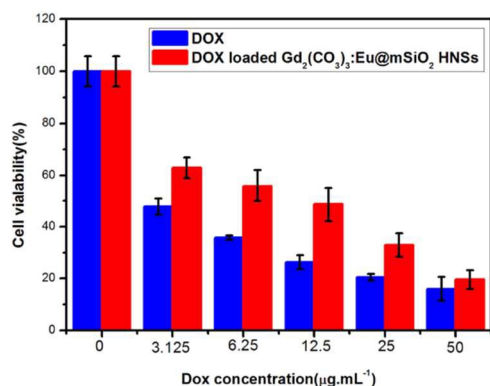
Figure.11 In vitro cytotoxicity of free DOX (blue) and DOX loaded $Gd_2(CO_3)_3$:Eu@mSiO$_2$ HNSs（red）

Conclusions

In summary, we have successfully prepared the well-dispersed mesoporous silica coated $Gd_2(CO_3)_3$:Eu HNSs by a template-directed method with silica NSs as the template. It showed both excellent fluorescence and magnetic properties and thus could be used as a dual-imaging agent for optical/MR imaging. In addition, $Gd_2(CO_3)_3$:Eu @mSiO$_2$ HNSs showed pH-dependent DOX release property, indicating its potential application in antitumor drug delivery. The efficient optical and MR imaging capabilities, as well as the hollow structure of $Gd_2(CO_3)_3$:Eu @mSiO$_2$ HNSs make it a promising platform for simultaneous bioimaging and drug delivery.

Acknowledgments

Notes and references

a Jiangxi Key Laboratory of Organic Chemistry, Jiangxi Science & Technology Normal University, Nanchang, 330013, China
b College of biology, Jiangxi Normal University, Nanchang 330022, China
c College of Chemistry, Nanchang University, Nanchang 330031, China
* Corresponding Author: Prof. Dr. Qiang Xiao and Prof. Dr. YongXiu Li
Fax: +86-791-83815183; tel.: +86-791-83815183. E-mail:Qiang Xiao@tsinghua.org.cn, yxli@nuc.edu.cn;

1   L. Cheng , K. Yang , Y. Li , J. Chen , C. Wang , M. Shao , S. T. Lee , Z. Liu, Angew. Chem. Int. Edit., 2011, 50, 7385-7390.

2   H. Gong, Z. L. Dong, Y. M. Liu, S. N. Yin, L. Cheng, W. Y. Xi, J. Xiang, K. Liu, Y. G. Li, Z. Liu, Adv. Funct. Mater., 2014, 24, 6413-6413.

3   L. J. A, W. Bi, L. Peng, L. Huang, C. X. Yue, D. Y. Gao, C. L. Wu, W. Su, Nanoscale., 2014, 6,10710-10716.

4   T. Kim, E. Momin, J. Choi, K. Yuan, H. Zaidi, J. Kim, M. Park, N. Lee, M. T. McMahon, A. Quinones-Hinojosa, J. W. M. Bulte, T. Hyeon, A.A. Gilad, J. Am. Chem. Soc., 2011,133, 2955-2961.

5   J. Zhang, Y. H Wang, Z. G Xu, H. X Zhang, P. Y Dong, L. N Guo, F. H. Li, S. Y Xin and W. Zeng, J. Mater. Chem. B, 2013, 1, 330-338.

6   I. F. Li, C. H. Su, H. S. Sheu, H. C. Chiu, Y. W. Lo, T. W. Lin, J. H. Chen, C. S. Yeh, Adv. Funct. Mater., 2008, 18, 766-776.

7   Y. H. Han, S. L. Gai, P' A. Ma, L. Z. Wang, M. L. Zhang, S. H Huang, P. P Yang, Inorg. Chem., 2013, 52, 9184-9191.

8   W. R. Zhao, H. R. Chen, Y. S. Li, L. Li, M. D. Lang, J. L Shi. Adv. Funct. Mater., 2008, 18, 2780-2788.

9   G. X. Yang, S. L. Gai, F. Y. Qu, and P. P. Yang, ACS Appl. Mater. Interfaces., 2013, 5, 5788-5796

10   T. Kim, N. Lee, Y. I. Park, J. W. Kim, J. Y. Kim, E. Y. Lee, M. Y. Yi, B-G Kim, T. W. Hyeon, T. Y. Yu, H. B. Na, RSC Adv., 2014, 4, 45687-45695.

11   D. M. Yang, P'A. Ma, Z. Y. Hou, Z. Y. Cheng, C. X. Li, J. Lin, Chem. Soc. Rev., 2015, 44, 1416-1448.

12   F. He, P. P. Yang, D. Wang, C. X. Li, N. Niu, S. L. Gai, and M. L. Zhang. Langmuir., 2011, 27, 5616-5623

13   H. P. Singh, S. Mitra, R. K. Sharma, RSC Adv., 2014, 4, 61028 -61035.

14   Z. H. Xu, Y. Cao, C. X. Li, P'A. Ma, X. F. Zhai, S. S. Huang, X. J. Kang, M. M. Shang, D. M. Yang, Y. L. Dai and J. Lin, J. Mater. Chem., 2011, 21, 3686-3694.

15   M. L. Debasu, A. Duarte, S. L. C. Pinho, F. G. C. Geraldes, L. D. Carlos, J. Rocha, Nanoscale, 2012, 4, 5154-5162.

16   Z. G. Yi, W. Lu, C. Qian, T. M. Zeng, L. Z. Yin, H. B. Wang, L. Rao, H. R. Liu, S. J. Zeng, Biomater. Sci., 2014, 2, 1404-1411.

17   W. Ren, G. Tian, L. J. Zhou, W. Y. Yin, L. Yan, S. Jin. Nanoscale, 2012, 4, 3754-3760.

18   Y. L. Deng, H. Wang, W. Gu, S. Li, N. Xiao, C. Shao, Q. Y. Xu, L. Ye. J. Mater. Chem. B, 2014, 2, 1521-1529.

19   M. He, P. Huang, C. L. Zhang, H. Y. Hu, C. C. Bao, G. Gao, R. Heand, D. X. Cui, Adv. Funct. Mater., 2011, 21, 4470-4477.

20   S. A. Shivashankar, S Majeed, Rapid, J. Mater. Chem. B, 2014, 2, 5585-5593.

21   Y. Gao, Q. Zhao, Q. Fang, Z. H. Xu, Dalton Transactions, 2013, 42, 11082-11091.

22   S. P. Fricker, Chem. Soc. Rev., 2006, 35, 524-533.

23   L. J. Zhou, W. Y. Yin, W. L. Ren, Z. J. Gu, L. Wei, S. Jin. New. J. Chem., 2012, 36, 2599-2606.

24   Y. L. Wu, X. Z. Xu, Q. Tang, Y. X. Li, Nanotechnology, 2012, 23, 205103-25109.

25   Y. Gao, M. M. Fan, Q. H. Fang, F. Yang, New. J. Chem., 2014, 38,146-154.

26   Q. Ji, J. P. Hill, K. Ariga, J. Mater. Chem. A., 2013, 1, 3600-3606.

27   S. H. Wu, Y. Hung, C. Y. Mou. Chem. Mater., 2013, 25(3): 352-364.

28   K.Y. J. Son, H-J. Yoon, J-H. Kim, W-D. Jang, Y. Lee, W-G. Koh, Angew. Chem.Int. Ed., 2011, 50, 11968-11971.

29   S. H. Tang, X. Q. Huang, X. L. Chen , N. F. Zheng, Adv. Funct. Mater., 2010, 20, 2442-2447.

30   R. W. Stöbe, A. Fink, E. Bohn, J. Colloid. Interface. Sci., 1968; 26, 62-69.

31   F. Y. Liu, X. X. He, L. Liu, H. P. You, H. M. Zhang, Z. X. Wang, Biomaterials, 2013, 34, 5218-5225.

32   S. L. Gai, P. P. Yang, C. X. Li, W. X. Wang, Y. L. Dai, N. Niu, J. Lin. Adv. Funct. Mater. 2010, 20, 1166-1172.

33   G. Tian, Z. J. Gu, X. X. Liu, L. J. Zhou, W. Y. Yin, L. Yan, S. Jin, W. L. Ren, G. M. Xing, S. J. Li, and Y. L. Zhao. J. Phys. Chem. C., 2011, 115, 23790-23796.

34   Y Wu, D M Yang, X J Kang, P A Ma, S S Huang, Y Zhang, C X Li, J Lin. Dalton Transactions, 2013, 42(27):9852-9861.
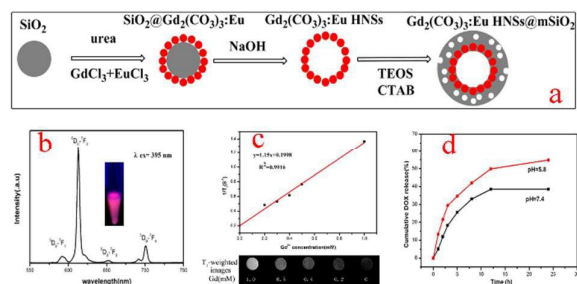
The efficient optical/MR imaging capabilities, and the hollow structure make $Gd_2(CO_3)_3$:Eu @mSiO$_2$ a promising platform for simultaneous bioimaging and drug delivery.